Friction **4**(3): 266–276 (2016)
DOI 10.1007/s40544-016-0125-7
ISSN 2223-7690
CN 10-1237/TH

RESEARCH ARTICLE

The validity of the Reynolds equation in spool valve analysis considering cavitation

Sung-Ho HONG, Kyung-Woong KIM*

School of Mechanical, Aerospace & Systems Engineering, Korea Advanced Institute of Science and Technology, 291 Daehak-ro, Yuseong-gu, Daejeon 305-701, Republic of Korea

Received: 20 June 2016 / Revised: 22 August 2016 / Accepted: 28 August 2016

Abstract: The purpose of this research is to investigate the validity of the Reynolds equation in spool valve analysis under cavitation. This study is carried out for a laminar and isothermal flow between a sleeve and spool with grooves. The pressure and lateral force obtained from the Reynolds equation and the Navier-Stokes equation are compared with variations of aspect ratio, cross sectional area, and number of grooves. The cavitation phenomenon is considered by using a cavitation model in the Navier-Stokes equation and the Reynolds cavitation boundary condition in the Reynolds equation. A large difference of more than 20% is found between the equations for a lateral force of spool valve with many grooves. It was found that the Reynolds equation is not suitable for calculation of a lateral force of the spool valve with multiple-grooves of which the width and depth are even larger than the clearance under cavitation.

Keywords: validity; Reynolds equation; Navier-Stokes equation; spool valve; cavitation

1 Introduction

Spool valves are used in many modern hydraulic systems to maintain the accurate movement of actuators. However, a spool-type directional control valve has a particular problem known as hydraulic lock. The problem occurs when an uneven pressure distribution surrounding the spool in the clearance between the spool and sleeve causes the spool to move sideways and out of its centered position. Contact between the spool and sleeve causes an increase of friction, and the spool is eventually blocked inside the sleeve. Lateral force is closely related to the problem. When the lateral force is too large, the spool is biased to the inner wall of the sleeve, and contact occurs.

To improve the problem, circumferential grooves balancing the uneven pressure distribution in the radial clearance are generally applied to the spool lands. Researchers and designers of hydraulic valves have attempted to find the reasons and solutions for the problem [1].

In these previous studies, the Reynolds equation was commonly used to investigate the lubrication characteristics of the spool valve. The applicability of the Reynolds equation is questionable in spool valve analysis because cavitation often occurs in the grooves and the depth of the groove is much higher than the clearance in most cases. Moreover, in these conditions, it is reported that some of the assumptions used in the Reynolds equation are not valid [2]. Therefore, it is important to investigate whether the Reynolds equation is valid in simulating the spool valve. However, no evaluation has been performed on the applicability of the Reynolds equation in spool valve analysis.

In recent years, similar studies have typically performed by comparing pressure distribution, maximum pressure, load capacity, friction force or friction coefficient acquired by the Navier-Stokes equation (CFD analysis) with those obtained by the Reynolds equation in other hydraulic systems [3–10]. The results

* Corresponding author: Kyung-Woong KIM.
E-mail: skymeche@kaist.ac.kr

List of symbols

Fl	Lateral force	p_{sat}	Saturation pressure
$(Fl_{RE}-Fl_{N\text{-}S})/Fl_{N\text{-}S}$ %	Lateral force ratio	u_0	Sliding speed of sleeve
K	Aspect ratio of groove	r, θ, z	Cylindrical coordinate
N-S	Navier-Stokes equation	r_0	Radius of sleeve
RE	Reynolds equation	r_1	Radius of spool
R_c	Vapor generation rate term	v_{ch}	Characteristic velocity
R_e	Vapor condensation rate term	v_m	Mass-averaged velocity
V	Total volume	$v_{r,k}$	Relative velocity for phase k
V_k	Volume of phase k	α	Tilting angle of spool
f_k	Mass fraction of phase k	α_k	Volume fraction of phase k
h_2	Depth of groove	γ	Effective exchange coefficient
l	Length of spool	μ	Viscosity of oil
l_1	Distance from edge to first groove	μ_m	Viscosity of mixture
l_2	Width of groove	ρ	Density of oil
l_3	Distance between groove	ρ_m	Density of mixture
n	Number of groove	σ	Surface tension coefficient of lubricant
n_0	Normal direction at film rupture boundary	g	Non-condensable gas
		l	Liquid
p	Pressure	v	Vapor
p_0, p_r	Pressure condition at edge of spool		

were compared with a variation of the ratio of the roughness height (depth) of grooves or dimples to the film thickness (clearance). Through the comparison, they insisted that the Reynolds equation is valid in the range where the roughness height is less than or comparable to the clearance. In addition, the results acquired by the Navier-Stokes equation were compared with those by the Stokes equation [11–14].

Most of the problems dealt with in these previous studies focused on two-dimensional configurations. Generally, the results from an analysis of an object with a two-dimensional configuration were overestimated compared to those of an analysis of an object with a three-dimensional configuration. The analysis of the three-dimensional configuration should thus be performed to investigate the validity of the Reynolds equation.

It has been reported that the inertia effect [11–14] and method used to treat cavitation [15–17] cause a discrepancy between the results obtained by the governing equations. However, this study does not consider the effects of the variation of the Reynolds number. Therefore, the validity of the Reynolds equation in the spool valve is investigated in the range of a low Reynolds number below 3 to minimize the inertia effect of fluid.

Most of the previous researches on the validity of the Reynolds equation were concerned with the micro scale dimples or grooves of an infinitely slider bearing [5, 7, 10–13]. Moreover, the cavitation phenomenon which occurs in grooves or dimples was neglected or treated with a simplistic approach such as the half Sommerfeld condition [3, 7, 10, 11, 13, 14]. However, to accurately evaluate the validity of the Reynolds equation in the problems, the cavitation phenomenon and three-dimensional configuration need to be considered.

In this study, to estimate the validity of the Reynolds equation in the spool valve analysis under cavitation, an analysis of a three-dimensional configuration of the spool valve is performed to consider the circumferential flow of the spool, and the cavitation phenomenon is considered by using a cavitation model in the Navier-Stokes equation and Reynolds cavitation

boundary condition in the Reynolds equation. The pressure distribution and lateral force acquired by the Navier-Stokes equation (CFD analysis) are compared with those obtained by the Reynolds equation.

2 Numerical model and numerical method

A real spool valve system has spool with several spool lands, as shown in Fig. 1(a). In this study, the geometry of the spool valve is simplified. Figure 1(b) shows a schematic of the spool valve used for numerical analysis. The spool with a length l and radius r_1 is placed inside a sleeve with a radius r_0. The spool is tilted at an angle α. The sleeve moves at a velocity of u_0 in the z direction while the spool is stationary. The pressure at both sides of the domain is thus constant as p_0 and p_r, respectively. Figure 1(c) shows the groove region. The aspect ratio of groove K is the ratio of groove depth h_2 over the groove width l_2. The depth and width of grooves are much larger than the clearance in the general spool valve. In this study, the difference between the results is

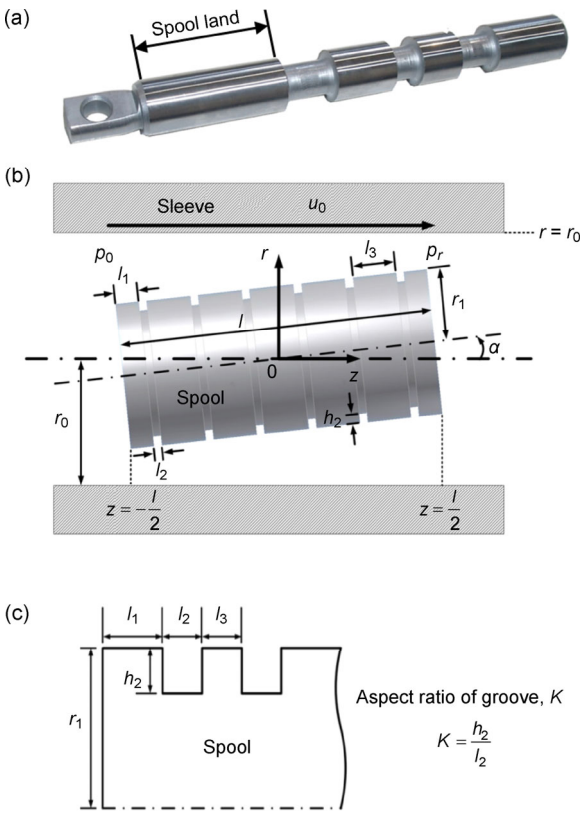

Fig. 1 Spool valve: (a) spool, (b) schematic of spool valve with groove, and (c) aspect ratio of groove.

calculated with the variation of the cross sectional area of the groove, the aspect ratio of the groove, and the number of grooves according to the governing equations. The saturation pressure, boundary pressure condition, and sliding speed are shown in Table 1 and the properties of the working fluid and the geometry of the spool valve are shown in Tables 2 and 3, respectively. "Oil" refers to the liquid-state of the lubricant and "oil-vapor" refers to the vapor state transformed from the lubricant of the liquid state.

Table 1 Pressure condition & sliding speed.

Pressure condition	p_0, p_r (Pa)	0
	p_{sat} (kPa)	−50
Sliding speed	u_0 (m/s)	3

Table 2 Properties of working fluid.

	Oil	Oil-vapor
Density (kg/m^3)	962	0.02556
Viscosity (kg/(m·s))	0.013468	1.256×10^{-5}
Surface tension (N/m)	0.0378	

Table 3 Geometries of spool valve.

r_0 (mm)	7.51
r_1 (mm)	7.5
l (mm)	20
l_1 (mm)	1.5
l_2 (mm)	0.1, 0.2, 0.3, 0.4, 0.5
l_3 (mm)	0.5
K	0.4, 1, 1.4
α (degree)	–0.0228
n (number of grooves)	2, 4, 8, 16

The evaluation of the validity of the Reynolds equation is performed by comparing the pressure distribution and lateral force obtained by numerical approach using the Reynolds equation (RE method) and computational fluid dynamics analysis using the Navier-Stokes equation (CFD method).

The Navier-Stokes equation is solved using commercial CFD software (FLUENT 6.3). The computational domain is meshed using the GAMBIT (version 2.3.16) pre-processor with the CFD method. A hexahedral grid is employed. Through testing mesh independence, it is verified that the pressure distribution rarely

changed above 1% error for various meshes in all cases when the fine mesh is applied to the domain as shown in Fig. 2(a). The left side of the domain is set as the pressure inlet and the right side is set as the pressure outlet.

The sleeve wall is set as the moving wall at a speed of u_0 in the z direction and the spool wall is set as the stationary wall. The no-slip boundary condition is assumed at the walls, and the pressure at the inlet and outlet boundaries of the spool valve is set to atmospheric pressure. FLUENT uses a finite volume method to convert the governing equations to algebraic equations that can be solved numerically.

The residual definitions are used for judging convergence. The criterion requires the residuals to decrease to 10^{-6} for the continuity equation, velocities, and volume fraction of vapor. The cavitation model used in FLUENT [18] was developed by Singhal et al. [19] and it accounts for effects such as phase change, bubble dynamics, and non-condensable gases. This model is able to account for two phase flows, which are the compressibility of both the liquid and gas phases. Various types of cavitation models can be used

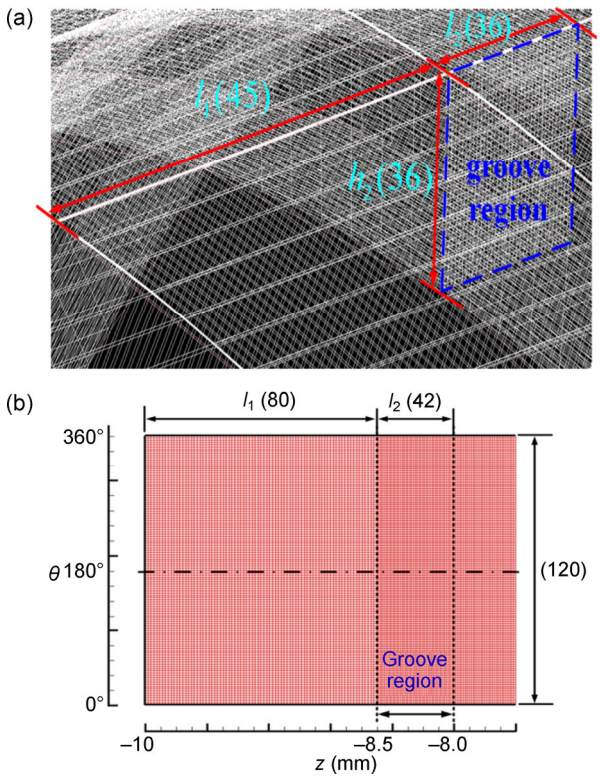

Fig. 2 Meshes near groove: (a) meshes in the CFD method and (b) meshes in the RE method.

in FLUENT. In this study, the cavitation is modeled by using mixture model from FLUENT. The mixture model solves the continuity equation for the mixture, the momentum equation for the mixture, the volume fraction equation for the secondary phase, the vapor mass fraction, and vapor transport equation, as well as the algebraic expression for relative velocities. The continuity equation for the mixture is

$$\nabla\cdot(\rho_{\mathrm{m}}\vec{v}_{\mathrm{m}})=0 \tag{1}$$

where ρ_{m} is the mixture density given by:

$$\rho_{\mathrm{m}}=\sum_{k=1}^{n}\alpha_k\rho_k \quad =\alpha_{\mathrm{v}}\rho_{\mathrm{v}}+\alpha_{\mathrm{g}}\rho_{\mathrm{g}}+(1-\alpha_{\mathrm{v}}-\alpha_{\mathrm{g}})\rho_{\mathrm{l}} \tag{2}$$

The mixture consists of three phases: liquid, vapor and non-condensable gas. The subscripts l, v and g donate liquid phase, vapor phase and non-condensable gas. α_k is the volume fraction of phase k and $\vec{v}_m$ is the mass-averaged velocity:

$$\vec{v}_{\mathrm{m}}=\frac{\sum_{k=1}^{n}\alpha_k\rho_k\vec{v}_k}{\rho_{\mathrm{m}}} \tag{3}$$

The momentum equation for the mixture can be obtained by summing the individual momentum equation for all phases. It is expressed as

$$\begin{aligned}\nabla\cdot(\rho_{\mathrm{m}}\vec{v}_{\mathrm{m}}\vec{v}_{\mathrm{m}})=&-\nabla p+\nabla\cdot[\mu_{\mathrm{m}}(\nabla\vec{v}_{\mathrm{m}}+\nabla\vec{v}_{\mathrm{m}}^{T})]\\&+\rho_{\mathrm{m}}\vec{g}+\nabla\cdot(\sum_{k=1}^{n_i}\alpha_k\rho_k\vec{v}_{\mathrm{r},k}\vec{v}_{\mathrm{r},k})\end{aligned} \tag{4}$$

where n_i is the number of phases and μ_{m} is the viscosity of the mixture:

$$\mu_{\mathrm{m}}=\sum_{k=1}^{n}\alpha_k\mu_k \tag{5}$$

$\vec{v}_{\mathrm{r},k}$ is the relative velocity for phase k:

$$\vec{v}_{\mathrm{r},k}=\vec{v}_k-\vec{v}_{\mathrm{m}} \tag{6}$$

A vapor transport equation governs the vapor mass fraction, f_{v}, given by:

$$\nabla\cdot(\rho_{\mathrm{m}}\vec{v}_{\mathrm{v}}f_{\mathrm{v}})=\nabla\cdot(\gamma\nabla f_{\mathrm{v}})+R_{\mathrm{e}}-R_{\mathrm{c}} \tag{7}$$

where γ is the effective exchange coefficient and R_{e} and R_{c} are the vapor generation and condensation

rate terms, respectively. The rates are functions of the instantaneous, local static pressure and are given by:

$$R_e = C_e \frac{v_{ch}}{\sigma} \rho_l \rho_v \sqrt{\frac{2(p_{sat} - p)}{3\rho_l}} (1 - f_v - f_g) \quad for \quad p < p_{sat} \tag{8}$$

$$R_c = C_c \frac{v_{ch}}{\sigma} \rho_l \rho_v \sqrt{\frac{2(p - p_{sat})}{3\rho_l}} f_v \quad for \quad p > p_{sat} \tag{9}$$

where σ is the surface tension coefficient of the liquid, p_{sat} is the liquid saturation vapor pressure at the given temperature, C_e and C_c are empirical constants with the default values $C_e = 0.02$ and $C_c = 0.01$, respectively, and v_{ch} is a characteristic velocity, which is approximated by the local turbulence intensity:

$$v_{ch} = \sqrt{k} \tag{10}$$

where f_k is the mass fraction of phase k.

The connection between the volume fraction in Eq. (2) and the mass fraction in Eqs. (7)–(9) is:

$$\frac{1}{\rho_m} = \frac{f_v}{\rho_v} + \frac{1 - f_v}{\rho_l} \tag{11}$$

The first order upwind scheme is applied for discretization and the SIMPLE pressure-velocity coupling algorithm is adopted to rapidly obtain the precise solution.

Secondly, the two-dimensional Reynolds equation is used in this study. The Reynolds equation can be derived from the Navier-Stokes equation and continuity equation by applying the general assumptions.

$$\frac{\partial}{\partial z}\left(h^3 \frac{\partial p}{\partial z}\right) + \frac{1}{r_0^2} \frac{\partial}{\partial \theta}\left(h^3 \frac{\partial p}{\partial \theta}\right) = 6\mu u_0 \frac{\partial h}{\partial z} \tag{12}$$

where μ is the viscosity of the lubricant and h is the film thickness. The film thickness differs according to the control regions of calculation. For example, in the control region between the left edge of the spool and the first groove from the left edge of the spool, the film thickness can be defined as follows:

$$h = c - z\alpha \cos\theta \quad \text{for} \quad -\frac{l}{2} \le z < -\frac{l}{2} + l_1 \tag{13}$$

where c is the clearance in the case where the axis of the spool coincides with that of the sleeve.

In order to consider the cavitation phenomenon in the RE method, the Reynolds cavitation boundary condition is applied.

$$p = p_{sat}, \frac{\partial p}{\partial n_0} = 0 \tag{14}$$

where n_0 represents the outward normal vector to the film rupture boundary and p_{sat} is the saturation pressure of the lubricant.

In the RE method, the Reynolds equation is discretized using the finite difference method and is solved using the Gauss-Seidel method. The convergence for the Reynolds equation is judged from the relative error of pressure. The convergence is approved when the relative error reaches less than 10^{-6}.

$$\frac{\sum \left| p^{new} - p^{old} \right|}{\sum p^{new}} < 10^{-6} \tag{15}$$

A flow chart of calculation is presented in Fig. 3(a). Figure 3(b) shows the discontinuity in the film thickness

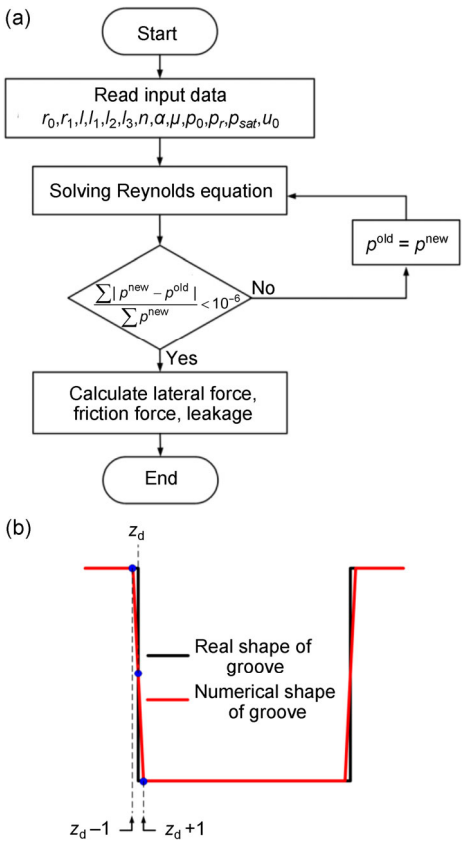

Fig. 3 RE method: (a) flow chart of the programming and (b) discontinuity in the film thickness.

in the z direction. For example, z_d is the location of the discontinuous fluid film thickness and coordinates z_d-1 and z_d+1 denote the position of immediately backward and immediately forward of the discontinuity line, respectively. At the position of discontinuity in the film thickness, the film thickness is expressed as Eq. (16).

$$h_{z=z_d}=\frac{h_{z=z_d-1}+h_{z=z_d+1}}{2} \tag{16}$$

Grid independency is carried out and it is verified that the solution change is below 1% error for the different meshes. The meshes near the groove are applied densely as shown in Fig. 2(b).

In this research, the pressure and lateral force are calculated using the CFD method and RE method, respectively. The lateral force is obtained by integrating the vertical components of the pressure over the spool surface, as shown in Eq. (17). The decrease in the absolute value of the lateral force can be related to the relief of the uneven pressure distribution surrounding the spool. In other words, a smaller absolute value of a dimensionless lateral force indicates a more effective mitigation of the uneven pressure distribution [20].

$$Fl=\int_{-l/2}^{l/2}\int_0^{2\pi} p\cos\theta r_1 \mathrm{d}\theta \mathrm{d}z \tag{17}$$

To investigate the validity of the Reynolds equation, the lateral force ratio is used. The ratios are presented in the form of normalized percentage. They are calculated on the basis of the results obtained by the Navier-Stokes equation (CFD method) because the results acquired by the CFD method are more precise than those by the RE method.

$$\frac{(\mathrm{Fl_{RE}}-\mathrm{Fl_{N\text{-}S}})}{\mathrm{Fl_{N\text{-}S}}}\%=\frac{(\mathrm{Fl_{RE}}-\mathrm{Fl_{N\text{-}S}})}{\mathrm{Fl_{N\text{-}S}}}\times 100 \tag{18}$$

where the subscripts N-S and RE represent the Navier-Stokes equation and the Reynolds equation, respectively.

3 Results and discussion

Figure 4(a) shows lateral forces with variation of groove width, l_2, and aspect ratio of groove, K, depending on numerical methods when the number of grooves, n is 2. The "N-S" and "RE" lines are shown for the results obtained from the CFD method and RE method, respectively. The lateral forces obtained by the CFD method are smaller than those obtained by the RE method. In addition, the lateral force decreases when the width of the groove increases for the same value of K. This is because the increment of the groove width refers to the increase of cross sectional area of the groove, and the increasing cross sectional area of the groove can help to release the uneven pressure distribution across the spool circumference. Figure 4(b) presents the lateral force ratios in the case where the number of grooves is 2. The lateral force ratios are less than 10%. When the number of grooves is 4, 8, and 16, the lateral force ratios are also calculated as shown in Figs. 4(c)–4(e), respectively. The difference of the lateral forces obtained by two governing equations increases as the number of grooves increases. Therefore, the evaluation with the Reynolds equation is not sufficient for calculation of lateral force in the case of a spool valve with multiple grooves.

The methods used to consider cavitation, pressure variation across film thickness, and the inertia of fluid have a significant influence on the difference of pressure distribution and lateral force according to numerical methods. This study focuses on the influence of pressure variation across the film thickness and the method used to consider cavitation as reasons for the difference in the results between the governing equations. However, the validity of the Reynolds equation in spool valve analysis is investigated in the range of a low Reynolds number of less than 3 in order to minimize the inertia effect of fluid in this study.

One of the assumptions used in deriving the Reynolds equation is that a negligible pressure variation occurs across the film thickness. Therefore, the pressure variation is investigated from the results acquired by the CFD method. When θ is 180°, the pressure change across the fluid film thickness is investigated at the center line and sidewalls of the first groove from the left edge of the spool as shown in Fig. 5. Figures 6–8 present the pressure variation across the film thickness in the case where the aspect ratio of the groove, K is 0.4, 1, and 1.4, respectively. The pressure variation in the r direction at the adjacent region of the

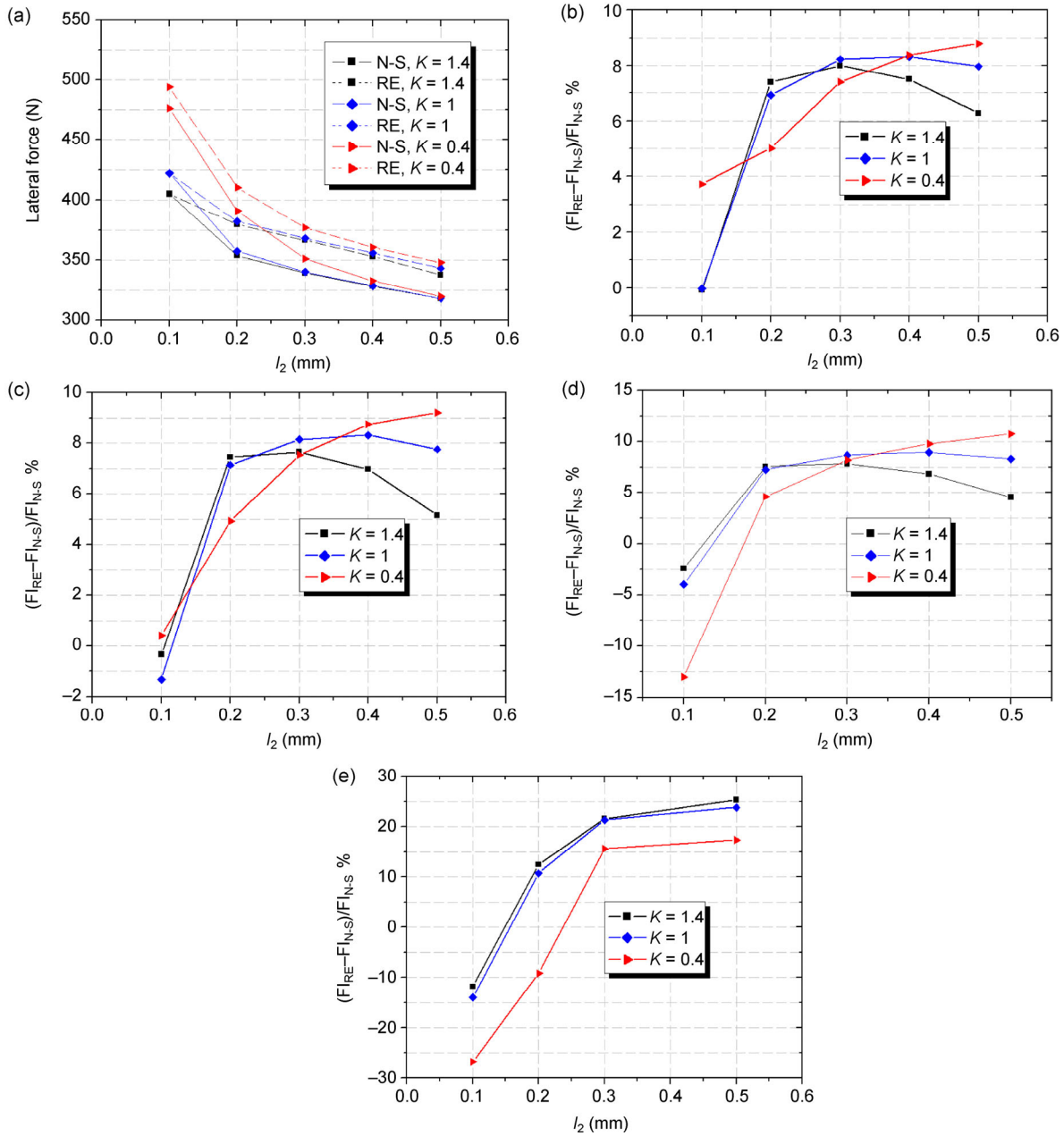

Fig. 4 Lateral force and lateral force ratio with variations of groove width, aspect ratio of groove, and number of groove: (a) lateral force (n = 2); (b) lateral force ratio (n = 2); (c) lateral force ratio (n = 4); (d) lateral force ratio (n = 8); (e) lateral force ratio (n = 16).

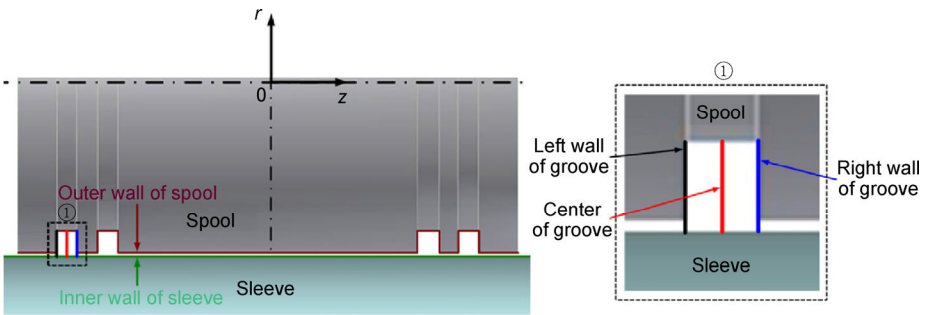

Fig. 5 Both sidewalls and center line of groove.

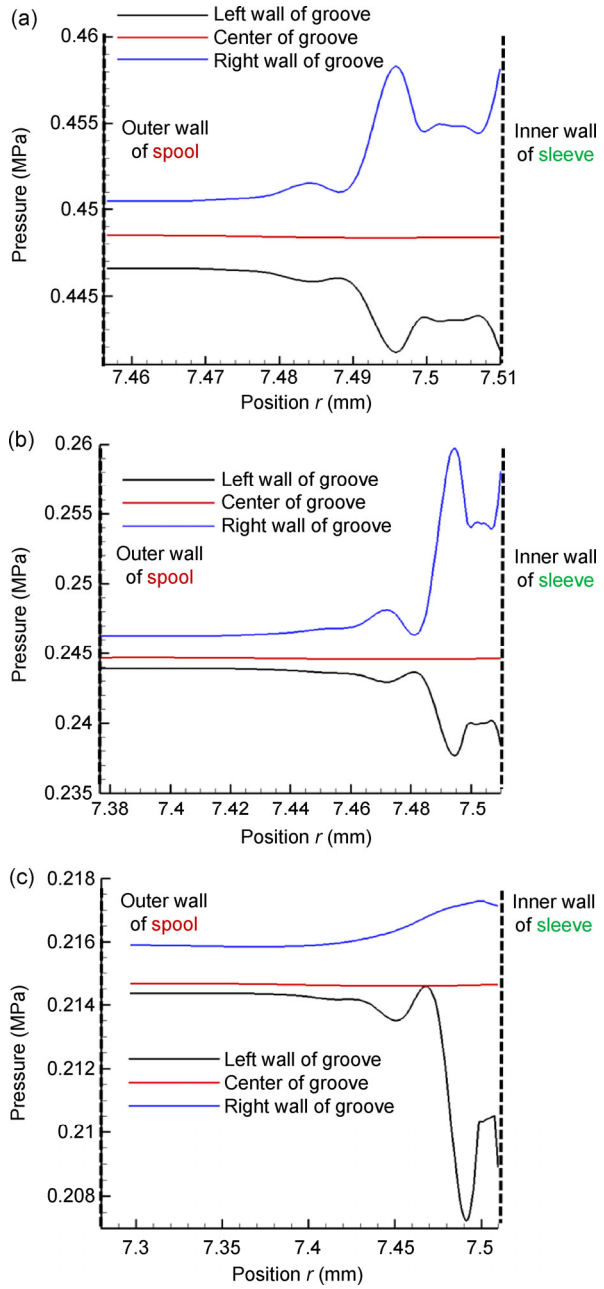

Fig. 6 Pressure variation across film thickness ($n = 2$, $K = 0.4$): (a) $l_2 = 0.1$ mm, (b) $l_2 = 0.3$ mm, and (c) $l_2 = 0.5$ mm.

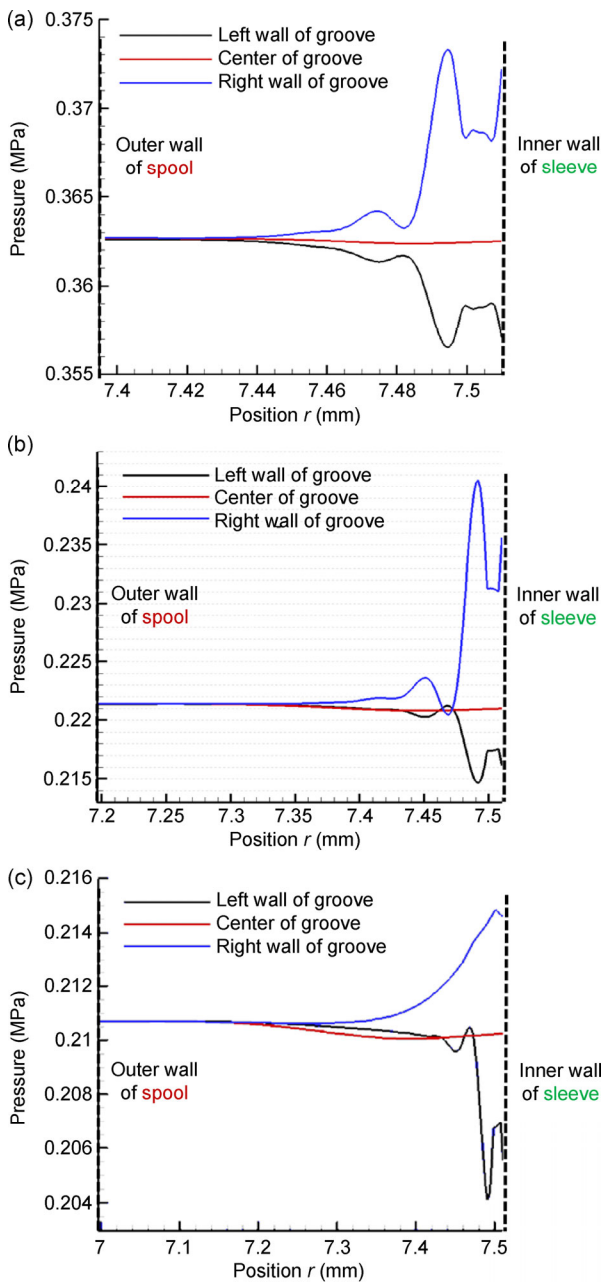

Fig. 7 Pressure variation across film thickness ($n = 2$, $K = 1$): (a) $l_2 = 0.1$ mm, (b) $l_2 = 0.3$ mm, (c) l_2=0.5 mm.

inner wall of the sleeve is higher than that at the adjacent region of the outer wall of the spool because the sleeve is moving part, not the spool. The pressure variation at the right wall of the groove is higher than that at the left wall of the groove in cases where the width of the groove, l_2 is 0.1 mm and 0.3 mm. However, in the case where the width of the groove is 0.5 mm, a relatively higher pressure variation at the left wall of the groove is shown. In cases where the depth of the groove is smaller than the width of the groove such as K=0.4, the pressure of the three positions (the two sidewalls and the center-line of the groove) is not the same at the adjacent region of the outer wall of the spool. On the other hand, there are regions where the pressure is the same or similar at the three positions in cases where the aspect ratio of the groove is 1 and 1.4. This is because the increased cross-sectional area of the groove facilitates to relieve uneven pressure

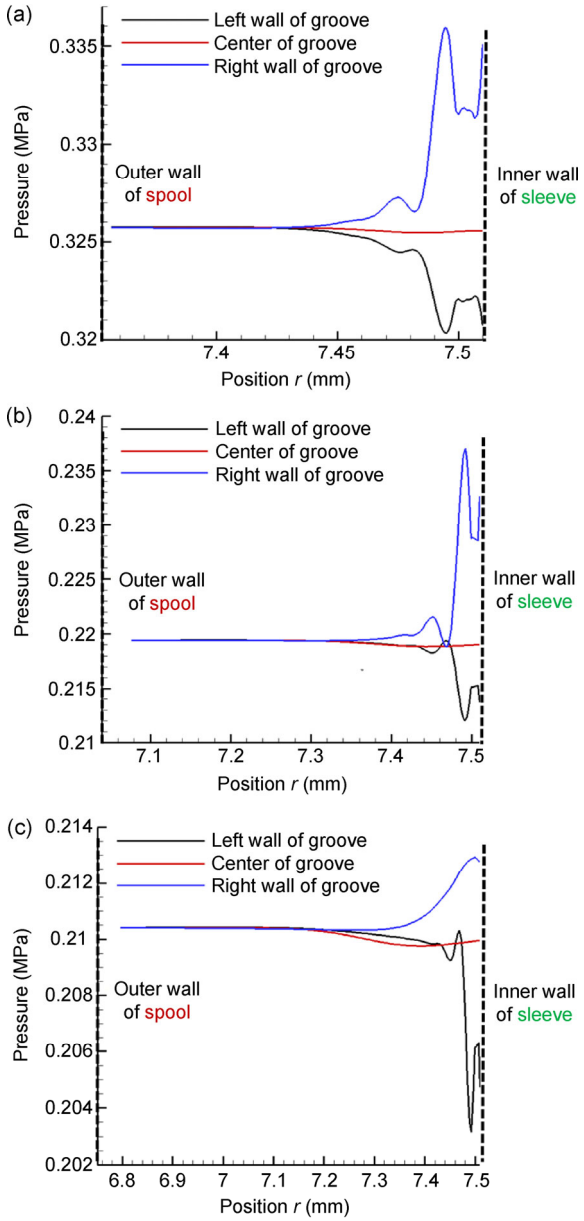

Fig. 8 Pressure variation across film thickness (n = 2, K = 1.4): (a) l_2 = 0.1 mm, (b) l_2 = 0.3 mm, and (c) l_2 = 0.5 mm.

distribution surrounding the spool in the circumferential direction. This is, when K is more than 1, the pressure of the three positions is the same or similar at the adjacent region of the outer wall of the spool due to occurrence of sufficient flow in the circumferential direction. Moreover, the pressure variation at the center-line of the groove is relatively higher in cases of K=1 and K=1.4 and marginal change of pressure occurs across the film thickness in the case of K = 0.4. Figures 9(a)–9(c) show the pressure variation across the film thickness in the cases of l_2 = 0.1 mm, l_2 = 0.3 mm, and l_2 = 0.5 mm, respectively when the number of grooves is 16 and the aspect ratio of the grooves is 1. Compared with the results shown in Fig. 6, the pattern of pressure variation is relatively smoother and the pressure is relatively lower due to the effect of multiple grooves. This is, when the number of the groove is 16, the relief function of uneven pressure distribution by the groove is more effective.

In previous studies, several different cavitation boundary conditions were applied to analysis of the lubrication problem in order to consider cavitation. Half Sommerfeld condition [21], Reynolds cavitation

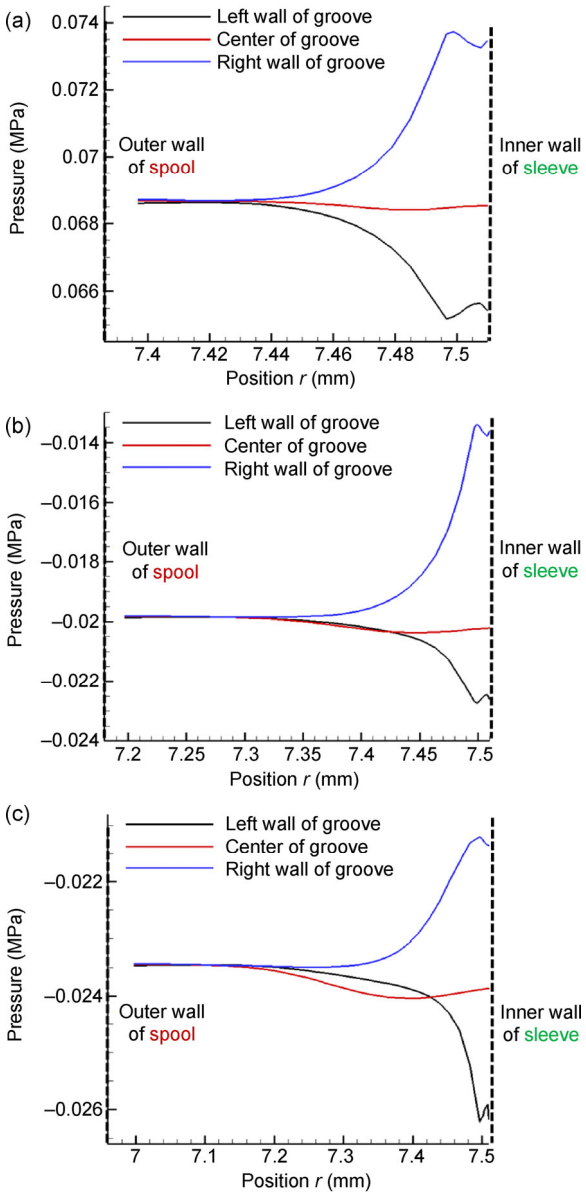

Fig. 9 Pressure variation across film thickness (n = 16, K = 1): (a) l_2 = 0.1 mm, (b) l_2 = 0.3 mm, and (c) l_2 = 0.5 mm.

boundary condition [15, 16] and JFO (Jakobsson-Floberg-Olsson) condition [15, 17] in a p-θ model are usually utilized in the analysis when using the Reynolds equation. And several cavitation models [19, 22, 23] in CFD analysis are also used.

The efficiency and accuracy of numerical analysis of the lubrication problem are important issues. As a rule, the analysis using the Reynolds equation is efficient in terms of time while the results of the CFD analysis using the Navier-Stokes equation are more precise but more time is needed to calculate the same problem. While the JFO condition is more accurate than the Reynolds cavitation boundary condition or the half Sommerfeld condition, it can be relatively time-consuming. In terms of efficiency and accuracy, cavitation is considered by using a cavitation model in the CFD method and by using the Reynolds cavitation boundary condition in the RE method. The RE method used in this present study does not satisfy mass conservation in the cavitation area and is known to underestimate the cavitation area [17]. Therefore, significant difference arises between the pressures calculated by the two methods. Especially, a distinct difference of pressure is observed near the groove region.

Figure 10 shows the pressure distributions in the z direction according to the different numerical methods, depth of groove, and width of groove (n = 2, K = 1, θ = 180°). The pressure distribution pattern calculated by the two numerical methods is similar, but a different pressure distribution is observed near the groove region. The difference near the groove region arises from the discrepancy of pressure distribution and maximum pressure. The maximum pressure obtained by the RE method is higher than that by the CFD method.

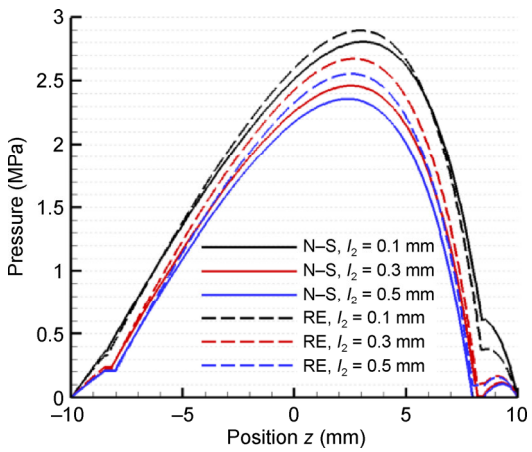

Fig. 10 Pressure distribution with variation of groove width and governing equations (K = 1, n = 2, θ = 180°).

It is believed that the difference of pressure depends on the method used to consider cavitation and whether or not the pressure variation across the film thickness is neglected. Furthermore, the difference of pressure distribution contributes to the discrepancy of pressure distribution and lateral force according to the numerical method used.

4 Conclusions

This study investigated the validity of the Reynolds equation in spool valve analysis under cavitation. The three-dimensional configuration of spool valve and the cases where the depth and the width of the groove were much higher than the clearance were considered in this research. The cavitation phenomenon was considered by using the Reynolds cavitation boundary condition in the RE method and the cavitation model in the CFD method.

The pressure and lateral force obtained by the RE method were compared with those by the CFD method with variation of aspect ratio, cross sectional area, and number of grooves. Through the comparison of results acquired by the two numerical methods, the following conclusions were found:

1. The difference in lateral forces obtained between the RE method and the CFD method increases as the number of grooves increases. In the case where the number of grooves is 16, a significant difference of lateral force of more than 20% is observed. Therefore, the evaluation with the Reynolds equation is not sufficient for the calculation of lateral forces in a spool valve with multiple grooves.
2. It is believed that the difference in the methods used to consider cavitation and to consider whether or not pressure variation across the film thickness is neglected affects the pressure distribution. Finally, the difference of pressure distribution causes differences in the lateral force according to the numerical method.

Acknowledgments

This work was supported by the BK 21 Plus Project.

References

[1] Sasaki A, Yamamoto T. A review of studies of hydraulic lock. *Lubrn Eng* **49**: 585–593 (1993)

[2] Brajdic-Mitidieri P, Gosman A D, Ioannides E, Spikes H A. CFD analysis of a low friction pocketed pad bearing. *J Tribol* **127**: 803–811 (2005)

[3] Song D J, Seo D K, Shults W W. A comparison study between Navier-Stokes equation and Reynolds equation in lubricating flow regime. *Int J Kor Soc Mech Eng* **17**: 599–605 (2003)

[4] Guardino C, Chew J W, Hills N J. Calculation of surface roughness effects on air-riding seals. *ASME J Eng Gas Turbines Power* **126**: 75–82 (2004)

[5] Almqvist T, Larsson R. Some remarks on the validity of Reynolds equation in the modeling of lubricant film flows on the surface roughness scale. *J Tribol* **126**: 703–710 (2004)

[6] Dobrica M B, Fillon M. Reynolds model suitability in simulating Rayleigh step bearing thermohydrodynamic problems. *Tribol Trans* **48**: 522–530 (2005)

[7] Dobrica M B, Fillon M. About the validity of Reynolds equation and inertia effects in textured sliders of infinite width. *Proc IMechE* **223**: 69–78 (2009)

[8] Feldman Y, Kligerman Y, Etsion I, Haber S. The validity of the Reynolds equation in modelling hydrostatic effects in gas lubricated textured parallel surfaces. *J Tribol* **128**: 345–350 (2006)

[9] De Kraker A, Ostayen R A J, Rixen D J. A multiscale method modeling surface texture effects. *J Tribol* **129**: 221–230 (2007)

[10] Li J, Chen H. Evaluation on applicability of Reynolds equation for squared transverse roughness compared to CFD. *J Tribol* **129**: 963–967 (2007)

[11] Odyck van D E A, Venner C H. Stokes flow in thin films. *J Tribol* **125**: 121–134 (2003)

[12] Odyck van D E A, Venner C H. Compressible stokes flow in thin films. *J Tribol* **125**: 543–551 (2003)

[13] Sahlin F, Glavatskih S B, Almqvist T, and Larsson R. Two-dimensional CFD analysis of micro-patterned surfaces in hydrodynamic lubrication. *J Tribol* **127**: 96–102 (2005)

[14] Arghir M, Roucou N, Helene M, Frene J. Theoretical analysis of the incompressible laminar flow in macro-roughness cell. *J Tribol* **125**: 309–318 (2003)

[15] Ausas R, Ragot P, Leiva J, Jai M, Bayada G, Buscaglia G. The impact of the cavitation model in the analysis of microtextured lubricated journal bearing. *J Tribol* **129**: 868–875 (2007)

[16] Elrod H G, Adams M. A computer program for cavitation. In *First Leeds-Lyon Symposium on Cavitation and Related Phenomena in Lubrication*, *I. M. E., Mechanical Engineering*, New York, 1974: 37–41.

[17] Qiu Y, Khonsari M M. On the prediction of cavitation in dimples using a mass-conservation algorithm. *J Tribol* **131**: 041702-1~041702–11 (2009)

[18] FLUENT 6.3 User's Guide

[19] Singhal A K, Athavale M M, Li H, Jiang Y. Mathematical basis and validation of the full cavitation model. *J Fluids Eng* **124**: 617–624 (2002)

[20] Hong S H, Kim K W. A new type groove for hydraulic spool valve. *Tribol Int* **103**: 629-640 (2016)

[21] Etsion I, Burstein L. A model for mechanical seals with regular micro surface structure. *Tribol Trans* **39**: 677–683 (1996)

[22] Kunz R F, Boger D A, Stinebring D R,Chyczewski T S, Lindau J W, Gibeling H J, Venkateswaran S, Govindan, T R. A preconditioned Navier-Stokes method for two-phase flows with application to cavitation prediction. *Comput Fluids* **29**: 849–875 (2000)

[23] Lindau J W, Kunz R F, Boger D A, Stinebring D R, Gibeling H J. High Reynolds number, unsteady multiphase CFD modeling of cavitating flows. *J Fluids Eng* **124**: 607–616 (2002)

Sung-Ho HONG. He received his M.S. and Ph.D. degrees in the Department of Mechanical Engineering from Korea Advanced Institute of Science and Technology, Deajeon, Korea. He has currently worked on tribology at engine and machinery division in Hyundai Heavy Industries. His current research interests include bearing, machine condition monitoring system based on lubricant analysis in marine engines.